Experimental analysis on stochastic behavior of preswitching time in STT-MRAM

N. Yazigy, J. Postel-Pellerin, V. Della Marca, K. Terziyan, S. Nadifi, R.C. Sousa, P. Canet, G. Di Pendina

Experimental analysis on stochastic behavior of preswitching time in STT-MRAM

N. Yazigy[a,*], J. Postel-Pellerin[a], V. Della Marca[a], K. Terziyan[a], S. Nadifi[a], R. C. Sousa[b], P. Canet[a], G. Di Pendina[b]

[a] Aix Marseille University, CNRS, IM2NP, 13451 Marseille, France.
[b] SPINTEC, University Grenoble Alpes, CNRS, CEA-SPINTEC, CEA, 38000 Grenoble, France.

Abstract

In this paper we present an experimental study on the preswitching time of Spin-Transfer Torque Magnetic Random-Access Memory (STT-MRAM) with a resistance area R.A.~12Ω·μm², for both transitions, Anti-Parallel to Parallel state and vice versa. A set of measurements is carried out operating at different applied voltages and temperatures ranging from 25°C to 90°C. As main results of our analysis, we show the decrease of the preswitching time with temperature increase. The Arrhenius law enables the extraction of the activation energy required to switch the cell in both states. Finally, we establish the relevant state transition probabilities using the Weibull distribution that best fits our results. The Weibull parameters highlight the preswitching time stochasticity and the variability of the switching characteristics of the STT-MRAM device, useful in high reliability applications.

1. Introduction

Spin Transfer Torque Magnetic Random-Access Memory (STT-MRAM) technology, where the data storage is managed by the Magnetic Tunnel Junction (MTJ) nano-pillar, is a promising answer for next-generation of non-volatile (NV) memory compared to traditional embedded NV-Flash and volatile SRAM technologies. Indeed, it offers high density, in the range of SRAM, low cost, low power consumption, endurance greater than 10^{12} cycles, good data retention capabilities as well as scalability beyond tens of nanometers [1,2]. Many electronics companies have recently showcased the future of STT-MRAM technology to deliver industrial-grade microcontrollers, Internet of Things (IoT) and data-centric artificial intelligence devices [3,4,5,6,7]. The resistance of an MTJ device depends on the relative orientation of the magnetization of two ferromagnetic (FM) layers, the free layer (FL) and reference layer (RL). The switching mechanism is a consequence of the spin-dependent tunneling. It is quantified by tunnel magnetoresistance ratio (TMR) [1,7]. The FL magnetization direction can be changed either by applying a static magnetic field higher than the coercivity of the FL or by injecting a spin-polarized current through the device. The transverse component of the spin current gets absorbed in the FL, implying a torque on the magnetization of the FL known as the Spin Transfer Torque (STT) effect [8,9,10]. The two possible states are: the high-resistive state when an Anti-Parallel (AP) configuration is setup and the low-resistive state when a Parallel (P) configuration is setup, that usually represent the "1" and "0" logical states respectively. A High-Resolution Transmission Electron Microscopy (HRTEM) of the whole stack used in our study is shown in [11]. Magnetic switching is a stochastic process, where the probability of having the desired state is a function of applied voltage (V_A), temperature, and pulse width [12]. In this paper we study the dynamic behavior of the cell during the time before the start of the current/resistance state change called preswitching time (t_P). This parameter depends on the applied voltage and temperature. A previous study [13] on the preswitching time for the AP to P transition at room temperature, showed a large variability on t_P which seems random for a given V_A. This paper will focus on demonstrating the stochasticity of both transitions.

2. Experimental setup and results

2.1. Experimental setup

The stack of the STT-MRAM device used in this work is as described in [14]. The core of the p-MTJ is the FeCoB (reference)/MgO/FeCoB (storage layer)/cap layer stack as shown in Fig. 1. The p-MTJ has a

* Corresponding author. nicole.yazigy@im2np.fr.
Tel: +33 413 554 019

resistance area R.A.~12Ω·µm^2 and a diameter size ~ 90 nm.

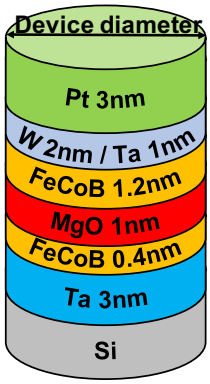

Fig. 1. Schematic drawing of top electrode half-MTJ stack [14]

Our characterization is performed on purpose to extract the switching parameters of the cell. The two switching operations, P to AP and AP to P, are obtained by respectively applying negative and positive bias voltage between -0.8V and 0.6V [13]. In this paper we show results carried out by quasistatic and dynamic characterizations. During the read phase, 0.1V bias is applied. The measurement of a low current through our cell indicates an AP state, thus a higher one indicates a P state. In order to limit and verify the variability each measurement has been repeated thirty times for each voltage at each temperature. The experimental setup is thus composed of both Source Measure Units (SMU) and Waveform Generator Fast Measurement Unit (WGFMU) implemented in the Keysight B1500 semiconductor device analyzer [13,15].

2.2. Quasistatic Measurements (QM)

Fig. 2 shows a Quasistatic cycling (30 cycles) for each temperature ranging from 25°C to 90°C, in order to define the key parameters of our cell such as R_P, R_{AP} and mean switching voltages. These parameters constitute guidelines for the pulsed dynamic measurements. In Fig. 2 we can notice that contrary to R_{AP}, R_P is almost constant thereby P state is more stable than AP state with temperature and voltage. It is also important to underline that the dispersion of switching voltages is greater during the AP to P transition than during the inverse transition from P to AP state.

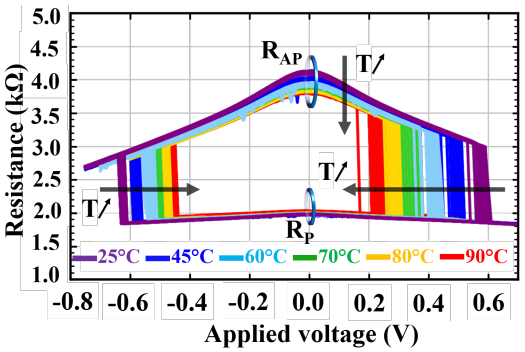

Fig. 2. R-V hysteresis characteristics cycled 30 times in the range of temperature from 25°C to 90°C.

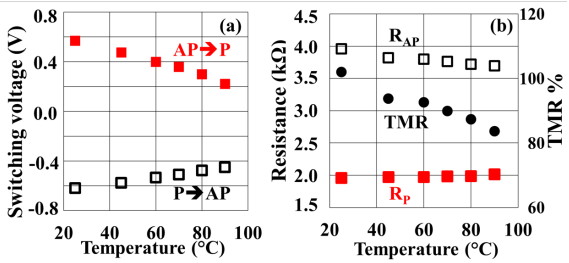

Fig. 3. (a) Mean values of switching voltages over 30 cycles for different temperatures, for both transitions, (b) extracted R_P and R_{AP} at 0.1V as well as TMR versus temperature.

In Fig. 3.a, one can notice the fast tendency towards 0V of the switching voltage during the switching to the P state, whereas for the reverse way this tendency is slower. The programming window is reduced by 44%, from 1.19V at 25°C to 0.67V at 90°C. Fig. 3.b. highlights that R_P is almost unaffected by temperature variations, while R_{AP} and TMR exhibit a clear decrease with the temperature increasing.

2.3. Pulsed Measurements (PM)

The extraction of the preswitching time (t_P) is performed by an efficient and smart write operation, that uses the parameters from the quasistatic measurements. The experimental protocol of writing phase consists in a voltage pattern with pulse widths from 100ns to 50s (an example is shown in Fig. 4).

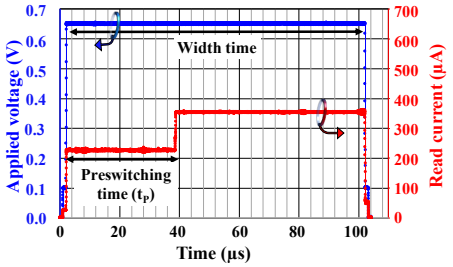

Fig. 4. Experimental result of the switching from an AP to P state by applying a voltage pattern while reading current.

The current flow in the MTJ is measured all along the waveform bias. The first and third pulses at 0.1V are used to measure the resistance before and after the switching. The width time enables the cell transition between the AP and the P states, while the current step-up allows to define the preswitching time (t_P). This method is used for all the data in the rest of the paper.

2.4. Temperature characterization

The measured preswitching times, presented in Fig. 5.a and Fig. 5.b, decrease for a given V_A when the temperature increases. We can also see that the transition from AP to P state in Fig. 5.b is more impacted by a temperature variation than the transition from P to AP state in Fig. 5.a , which agrees with the results obtained in the previous section. With this set of electrical characterizations, it is possible to extrapolate the data retention of the STT-MRAM device at each temperature for both switching states, by extending the trend lines and taking their intersection with the Y-axis, V_A=0V, not visible in the figure in order to preserve its visibility. At 25°C, the data retention of the P state is 10^{29}s while it is $5{\cdot}10^{13}$s for the AP state. At 90°C, these values decrease to $5{\cdot}10^{22}$s (P state) and $3{\cdot}10^{2}$s (AP state). This confirms that the P state is more stable, even at high temperature.

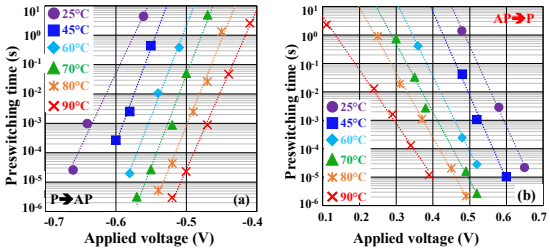

Fig. 5. Mean values over 30 measurements of preswitching times ($\underline{t_P}$), for different V_A and temperatures ranging from 25°C to 90°C for the transition (a) from P to AP state and (b) from AP to P state.

From our previous work [13] and based on the experimental results exhibited in Fig. 5, for a given temperature the relation between the preswitching time and the applied voltage is given by the Equation (1) :

$$t_P = t_{0P}.e^{-V_A/V_{0P}} \qquad (1)$$

Where t_P is the preswitching time, t_{0P} is the preswitching time at V_A=0V and V_{0P} is a voltage scale parameter. Therefore, we can also study the thermal stability by using this Equation 1 for different temperatures and applied voltages, in order to extract the activation energy Ea by linking the preswitching time to Arrhenius law expressed in Equation (2):

$$t_P \propto e^{Ea/kT} \qquad (2)$$

where Ea is the activation energy of the switching phase, k is the Boltzmann constant and T is the temperature in Kelvin. We plotted in logarithmic scale the preswitching times as a function of 1/kT for V_A ranging from -0.45V to -0.65V for the P to AP transition (Fig. 6.a) and 0.45V to 0.65V for the AP to P transition (Fig. 6.b).

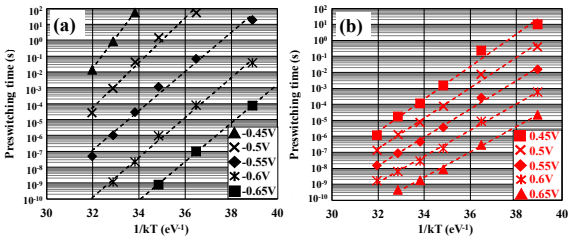

Fig.6. Preswitching time (t_P) for V_A ranging from (a) -0.45V to -0.65V (P to AP) and (b) 0.45V to 0.65V (AP to P) as a function of (1/kT).

The activation energy values are then extracted and presented in Fig. 7.

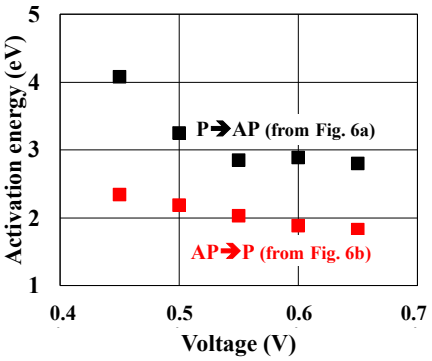

Fig. 7. The activation energies as a function of the absolute value of V_A, extracted from Fig.6 (a) from P to AP state and (b) from AP to P state

We can notice in Fig. 7 that for a given applied voltage the activation energy is always lower for the AP to P transition than for the P to AP one. This is coherent with the fact that the AP state is known to be less stable than P state [16,17]. We also notice that the activation energy slightly decreases with the applied voltage since less energy is required to reach the switch for high applied voltages [13]. For the P to AP transition at low applied voltage (V_A=-0.45V), the activation energy is higher (above 4eV) showing a different mechanism, probably due to self-heating of the device as evidenced in [18].

2.5. Stochasticity of MTJ switching

In order to study the stochastic behavior of the switching operations, we plot the measurement using the Weibull law (Equation (3)). The reason for choosing thirty consecutive measurements is to have a probability precision of the order of 3%, compatible with the Weibull distribution which is used to model the preswitching time (t_P) which has high variability suggesting random occurrence.

$$F(t_P) = 1 - e^{-(\frac{t_P - t_0}{\tau})^{\beta}} \quad (3)$$

where the scale parameter τ is the characteristic time-to-switch somewhat analogous to a "mean time to preswitching", β is the form factor or Weibull slope, that determines the shape of the distribution and t_0 is the position factor, corresponding to the smallest time giving a non-zero probability of switching [19]. The $\mathrm{Ln}(-\mathrm{Ln}(1 - F(t_P))$ plot, commonly known as the Weibit plot [20,21], is presented as marks in Fig. 8.

The three Weibull parameters β, t_0 and τ can be extracted from these experimental (marks) Weibit plots at 25°C for P to AP (Fig. 8.a) and AP to P (Fig. 8.b). Rearranging Equation (3) by using the appropriate logarithms, we obtain Equation (4) where the right-hand side represents the model plotted as lines in Fig. 8. The Weibull slopes β are given as well.

$$\mathrm{Ln}(-\mathrm{Ln}(1 - F(t_P)) = \beta \cdot \mathrm{Ln}(\frac{t_P - t_0}{\tau}) \quad (4)$$

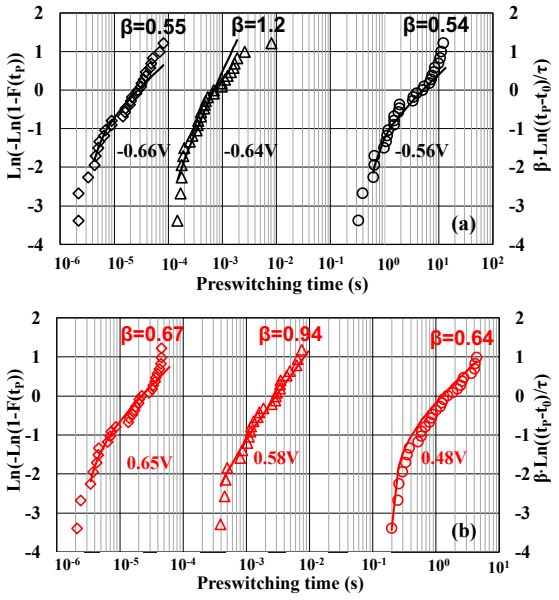

Fig. 8. Weibit plot of $\mathbf{t_P}$ for six different voltages of the switching (a) P to AP and (b) AP to P, at 25°C. "$\mathbf{Ln(-Ln(1 - F(t_P))}$": marks - measurements and "$\boldsymbol{\beta \cdot Ln(\frac{t_P - t_0}{\tau})}$": lines -Weibull model.

The concavity of the curves in Fig. 8 is due to the fact that the position parameter t_0 is not equal to 0 in our experiments and thus the linearity of the curves would be obtained when plotting them as a function of $(t_P - t_0)$ [22]. The position parameter t_0 is consequently important during the extraction procedure of the two other parameters τ and β.

For a fixed voltage and temperature condition, we show the corresponding Weibit plot for each experimental condition (voltage-temperature) and we calculate its tau parameter. In our set of experiments each tau parameter corresponds to the mean value of the measured preswitching time, as plotted in Fig. 9. The scale parameter τ is found to correspond to t_P as their relation is fitted by the equation $\tau = t_P$.

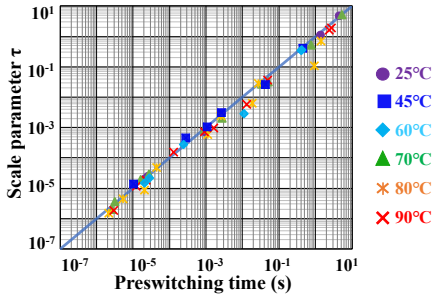

Fig. 9. Values of the scale parameter τ versus $\mathbf{t_P}$ in the range between 25°C and 90°C.

The form factor β is the most important factor of the Weibull distribution whose values are shown in Fig. 9.

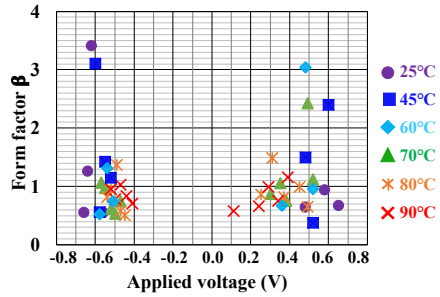

Fig. 10. Values of the form factor β versus V_A in the range between 25°C and 90°C.

Note that in the special case where β=1 the Weibull distribution becomes the single-parameter exponential distribution and the hazard function is a constant. In this case, the hazard rate is no longer a function of time and the phenomenon is considered to be stochastic [19,23,24,25]. We can notice that the values of β in Fig. 10 are mainly around 1, indicating a stochastic behavior of MTJ switching for these temperatures.

3. Discussion

The variation in the data retention shown in Fig. 5. can be explained by the fact that the P state is the natural state of our cell, thus the preferred or more stable state [16,17]. The transition toward the AP state is more difficult, less voltage is required in absolute value to pass from the AP to P state than to pass from the P to AP state. The data retention is therefore linked to this fact. Thus, the two intrinsic P and AP states have two different energy states with a single energy barrier characterizing the transition. The activation energy Ea values also show that even for a high voltage biasing condition (in absolute value) the transition from P to AP requires more energy than the reverse transition.
Concerning the Weibit plot, when the Weibit slope β is close to or equal to 1 this means the cell has a reasonably constant switching time rate indicative of a stochastic behavior of the switching transition. In addition, for higher applied voltages, β may increase [23] while it remains relatively independent of temperature [26]. β indicates that the cell is uncertain for a prediction during the state transition [27]. At high applied voltages (β>>1) the switching is very fast, the AP state is more and more unstable, and this prevented us from measuring t_P [28]. The Weibull distribution is generally used to express failure rates and evaluate the time-to-failure of devices, based on the bathtub curve. In our study it is applied to the preswitching time of STT-MRAM devices and enables to show that our devices are mainly in their useful life (with a stochastic switching probability and a constant "switching rate"). The methodology can be used during the development and the characterization of new devices to determine if they are in an early switching zone (decreasing "switching rate") and require a burn-in procedure or in a wear-out zone (increasing "switching rate") and is damaged.

4. Conclusion

In this paper we measured the preswitching times for AP to P and P to AP transitions using a dynamic method for different applied voltages and for temperature ranging from 25°C to 90°C. First, we extrapolated the cell data retention for both P and AP states, showing very good data retentions, even at high temperature. These temperature experiments also allowed the extraction of activation energies for AP to P and for P to AP transitions, using the Arrhenius law. The activation energy is always lower for the AP to P transition than for the P to AP one, which is coherent with the fact that the AP state is known to be less stable. Moreover, using the Weibull model, we highlighted the stochastic behavior of the STT-MRAM device switching dynamics for all the applied voltages and temperatures considered in this study.

Acknowledgements

This work was supported by the grant n°ANR-19-CE39-0010 overseen by the French National Research Agency (ANR).

References

[1] Apalkov D. et al., Spin-transfer torque magnetic random-access memory (STT-MRAM), Emerg. Technol. Comput., Syst. 9, 2, Article 13 ,2013, 35p.
[2] Sterpone L. and Violante M., "Analysis of the robustness of the TMR architecture in SRAM-based FPGAs," IEEE Transactions on Nuclear Science, vol. 52, no. 5 ,2005, pp. 1545-1549.
[3] Naik V. B. et al., Manufacturable 22nm FD-SOI Embedded MRAM Technology for Industrial-grade MCU and IoT Applications, 2019 IEEE International Electron Devices Meeting (IEDM).
[4] Golonzka O. et al., MRAM as Embedded Non-Volatile Memory Solution for 22FFL FinFET Technology, 2018 IEEE International Electron Devices Meeting (IEDM), 2018, pp. 18.1.1-18.1.4.
[5] Song Y. J. et al., Demonstration of Highly Manufacturable STT-MRAM Embedded in 28nm Logic, IEEE International Electron Devices Meeting (IEDM), 2018, pp. 18.2.1-18.2.4.
[6] Gallagher W. J. et al., 22nm STT-MRAM for Reflow and Automotive Uses with High Yield, Reliability, and Magnetic Immunity and with Performance and Shielding Options, IEEE International Electron Devices Meeting (IEDM), 2019, pp. 2.7.1-2.7.4.
[7] Alzate J. G. et al., 2 MB Array-Level Demonstration of STT-MRAM Process and Performance Towards L4 Cache Applications, IEEE International Electron Devices Meeting (IEDM), 2019, pp. 2.4.1-2.4.4.
[8] Sharma A. et al., Proposal for energy efficient spin transfer torque magnetoresistive random access memory device, Journal of Applied Physics, vol. 129, no.23, 2021.
[9] Brataas A. et al., Current-induced torques in magnetic materials, Nature Materials, vol.11, no. 5. Nature Publishing Group, 2012, pp. 372–381.
[10] Butler W. H. et al., Spin-dependent tunneling conductance of Fe/MgO/Fe sandwiches, Physical Review B - Condensed Matter and Materials Physics, vol. 63, no. 5, 2001, pp. 544161–5441612.
[11] Chatterjee J. et al. Physicochemical origin of improvement of magnetic and transport properties of STT-MRAM cells using tungsten on FeCoB storage layer. Applied Physics Letters, 2019, 114(9).
[12] Tan, J. L. Role of temperature, MTJ size and pulse-width on STT-MRAM bit-error rate and backhopping. Solid-State Electronics, 183 ,2021.
[13] Yazigy N. et al., Real-time dynamics in STT-MRAM switching. JEDS. 2022 (to be published)
[14] Chatterjee J., Sousa R. C., Perrissin N., Auffret S., Ducruet C., and Dieny B., Enhanced annealing stability and

perpendicular magnetic anisotropy in perpendicular magnetic tunnel junctions using W layer, Applied Physics Letters, vol. 110, no. 20, p. 202401, May 2017, doi: 10.1063/1.4983159.
[15] Aoyama H., B1500A Semiconductor Device Analyzer. [Online]. Available: www.keysight.com
[16] Devolder T., Le Goff A., Nikitin V. Size dependence of nanosecond-scale spin-torque switching in perpendicularly magnetized tunnel junctions. Physical Review B, 93(22), (2016).doi:10.1103/physrevb.93.224432
[17] Van Beek, S. Reliability Characterization of STT-MRAM Magnetic Memory. The Impact of Self-Heating. 2018.
[18] Van Beek et al. Impact of self-heating on reliability predictions in STT-MRAM. 2018 IEEE International Electron Devices Meeting (IEDM), 2018. doi:10.1109/iedm.2018.8614617
[19] Arthur J., Hallinan Jr., A Review of the Weibull Distribution, Journal of Quality Technology, 25:2, 85-93, 1993. doi: 10.1080/00224065.1993.11979431
[20] Park K. et al. Development of an advanced TDDB analysis model for temperature dependency. Electronics, 8(9), 2019, 942.
[21] McPherson, J. W. Reliability. Physics and Engineering: Time-to-failure modeling. Springer, 2010.
[22] Publishing, R. S. (n.d.). Location parameter of the weibull distribution, this issue's reliability basic. weibull.com -- Free Data Analysis and Modeling Resources for Reliability Engineering. Retrieved May 20, 2022, from https://www.weibull.com/hotwire/issue15/relbasics15.htm
[23] Pascale E. et al. Application of the Weibull distribution for the optimization of maintenance policies of an electronic railway signaling system. European Safety and Reliability Conference, 2017, 8p
[24] McCool, J. I. (2012). Using the weibull distribution: Reliability, modeling and Inference. Wiley.
[25] Prabhakar, M. D. N., Xie, M., Jiang, R. (2004). Weibull models. Wiley.
[26] Bedau, D., Liu, H., Sun, J. Z., Katine, J. A., Fullerton, E. E., Mangin, S., & Kent, A. D. (2010). Spin-transfer pulse switching: From the dynamic to the thermally activated regime. Applied Physics Letters, 97(26), 262502. doi:10.1063/1.3532960
[27] Panagopoulos G. et al. "Modeling of dielectric breakdown-induced time-dependent STT-MRAM performance degradation," 69th Device Research Conference, 2011, pp. 125-126.
[28] Tillie L. et al., "Data retention extraction methodology for perpendicular STT-MRAM," 2016 IEEE International Electron Devices Meeting (IEDM), 2016, pp. 27.3.1-27.3.4.